PAPER

Check for updates

Magnetic-assisted preparation and performance control of Fe₃O₄/PVDF gradient magnetic composites†

Miao Wang ⓘ * and Zhenming Zhang

In this study, a gradient Fe_3O_4/PVDF magnetic composite was prepared using magnetic-assisted template filling technology. The purpose of this study was to explore a simple, economical, and scalable method for preparing gradient magnetic composites. The structure and magnetic performance of the composite were studied, and the parameters that influenced the gradient magnetic properties of the material, such as magnetic intensity, magnet spacing, initial content of magnetic particles, and magnet movement speed, were investigated. The results showed that increasing magnetic intensity during the template filling process enhanced the electromagnetic force on the magnetic particles, resulting in a greater magnetic particle content gradient. The variation in magnet spacing affected the spatial magnetic field distribution, and increasing the magnet spacing increased the gradient of the magnetic intensity in the y-direction. The magnetic gradient of the Fe_3O_4/PVDF composite first decreased and then increased as the magnet spacing increased. Increasing the magnet movement speed enhanced the gradient of the magnetic intensity in the y-component but shortened the duration of the electromagnetic force. By adjusting these parameters, it is possible to regulate the structural and magnetic properties of the Fe_3O_4/PVDF composite. This work may have implications for research and application in related fields and promote the development and innovation of magnetic materials.

1 Introduction

As important functional materials, magnetic materials have a wide range of applications and are closely related to informatization, automation, mechatronics, and the national economy.[1–3] Traditional inorganic magnetic materials, such as ferrites, rare earth magnets, and aluminum–nickel–cobalt alloy magnets, have drawbacks such as high density, brittleness, large deformation, and difficulty in producing precision products.[4] The commonly used magnetic material Fe_3O_4 can exhibit magnetism under the influence of a magnetic field, but it does not retain magnetization after the magnetic field is removed. It has high saturation magnetization, superparamagnetism, and special force-responsive, biocompatible, chemical, and thermal properties, and has attracted widespread attention in the preparation of magnetic materials.[5,6] However, traditional single materials are no longer able to meet the demands of current industrial production. To solve this problem, magnetic composite materials, especially magnetic gradient materials, have gradually become a research hotspot and represent the future development trend.

In the forming process of magnetic composites, different base materials (inorganic or organic) can be selected according to actual needs.[7,8] Wang *et al.*[9] prepared ordered Co–Ni core–shell magnetic nanorod arrays using a two-step electrodeposition process, providing the possibility of adjusting appropriate coercivity at the nanoscale. Zhu *et al.*[10] achieved continuous and controllable adjustment of magnetic parameters by utilizing different bending radii of membranes. Li *et al.*[11] improved the magnetic performance of rare earth-based sintered composite magnets by adjusting the element distribution. Dong *et al.*[12] adjusted the magnetic properties of a seven-coordinated dysprosium(III) single-molecule magnet by manipulating the effect of positional isomer on the axial crystal field. Shang *et al.*[13] studied the modulation of multi-scale copper distribution on the magnetic properties of $Sm(CoFeCuZr)_z$ magnets.

Magnetic fields are ubiquitous in nature and find wide applications in materials forming, control of chemical reactions, modulation of magnetic nanoparticles, and adjustment of magnetic composite material properties. Researchers have combined magnetic fields with traditional micro/nano fabrication methods such as evaporation deposition, hydrothermal synthesis, and template synthesis, bringing new development opportunities for micro/nano materials. Vives[14] refined aluminum alloys using alternating current (AC) magnetic fields. Gavira *et al.*[15] found that a strong magnetic field of 7 Tesla can influence the nucleation and growth of tetragonal lysozyme

School of Mechanical Engineering, Northwestern Polytechnical University, Youyi West Road 127, 710072 Xi'an, China. E-mail: wmiao@mail.nwpu.edu.cn

† Electronic supplementary information (ESI) available. See DOI: https://doi.org/10.1039/d3ra08804a

crystals. Hu et al.[16] believed that magnetic fields can enhance the diffusion of Mo ions and promote the oriented growth of MoS_2, thereby improving its conductivity and lithium storage performance. Zhu et al.[17] applied a magnetic field during the hydrothermal preparation process of MnO_2 nanostructures and studied its influence on phase and morphology transitions. Hippo et al.[18] obtained highly oriented silicon arrays with a diameter of 100 nm and an aspect ratio of 160 using magnetic field-assisted anodization. Cui et al.[19] proposed a dynamic model to analyze the motion and mechanics of nanoparticles in magnetic fluids, providing a theoretical basis for describing the distribution evolution of magnetic particles under magnetic and flow fields. The oriented arrangement of magnetic nanoparticles provides a new option for manipulating material properties.

In recent years, gradient magnetic composites have become a hot topic of research, with scholars conducting extensive studies in theoretical design, preparation processes, performance modulation, and application fields. Shi et al.[20] carried out theoretical analysis on the magnetic energy harvester of functional gradient composite cantilevers to improve harvesting capacity and adjust resonance frequency. They established a theoretical model of magnetic-mechanical-electric (MME) effect for functional gradient composite cantilevers. Silva[21] created functional-level adhesive joints using polyurethane adhesive and iron microparticles, applying an appropriate magnetic field in the central region of the overlap area to form the functional-level adhesive joints. Mazur et al.[22] studied the self-assembly of magnetic nanoparticles on a flat nanocomposite surface with hidden magnetic patterns and demonstrated that the application of multilayer stamped media and the presence of magnetic field gradients can attract and organize superparamagnetic iron oxide nanoparticles into predefined regions. Phuoc and Ong[23] prepared NiFeW thin films using composition-gradient deposition technique and characterized their static and dynamic magnetic properties at different temperatures. Cabo et al.[24] synthesized component-gradient mesoporous composites of $NiO/NiCo_2O_4/Co_3O_4$ by controlling the reaction conditions and formulations during synthesis to achieve compositional gradients. Zhong et al.[25] used a hybrid deposition method combining oblique gradient composition sputtering and gradient composition sputtering techniques to prepare FeSiAl–Al_2O_3 films. Du et al.[26] deposited FeCoB films using a composition-gradient sputtering method and studied the static and high-frequency magnetic properties of FeCoB/Ru/FeCoB trilayer films.

Currently, most of the researches on magnetic gradient materials are focused on the field of inorganic materials. However, the development of this field has been limited due to the disadvantages of inorganic materials, such as high density, susceptibility to deformation, and the requirement for high processing temperatures. At the same time, polymer materials, as one of the three major materials alongside metals and ceramics, are playing an increasingly important role. The use of mature polymer processing methods and equipment to prepare polymer-based gradient materials will bring new opportunities for the research and application of polymer-based composites.[27]

Therefore, this study uses polymers as the matrix material and combines the magnetism of ferric oxide with polymers to produce polymer-based magnetic gradient materials. By describing the principles, steps, and experimental results of this method in detail, we aim to evaluate its feasibility and applicability in the field of gradient magnetic composites. Through this study, we hope to provide a more concise and efficient solution for the preparation of gradient magnetic composites, offer strong support for research and applications in related fields, and contribute to the advancement and innovation of magnetic materials.

2 Experimental

Fig. 1 demonstrates the formation process of gradient magnetic composites, which involves the application of both a magnetic field and a pressure field during the template filling process. The magnetic-assisted template filling device consists of two main components: a device for generating a moving magnetic field and a device for applying pressure to fill the template. The device for generating a moving magnetic field generates an electromagnetic force that causes magnetic nanoparticles to move in the direction of the magnetic field, resulting in a gradient in particle content along the direction of movement. The magnetic slurry system is a mixture of magnetic particles and fluid, and under the influence of an external magnetic field, the magnetic particles become magnetized and generate a magnetic force. The relationship between the magnetization strength (M) of the particles and the magnetic field strength (H) can be expressed as:[28]

$$M = \chi H \tag{1}$$

Here, χ represents the intrinsic magnetic susceptibility of the magnetic particles themselves, and H represents the spatial magnetic field in which the magnetic particles are located. Therefore, the magnetic field force acting on the magnetic
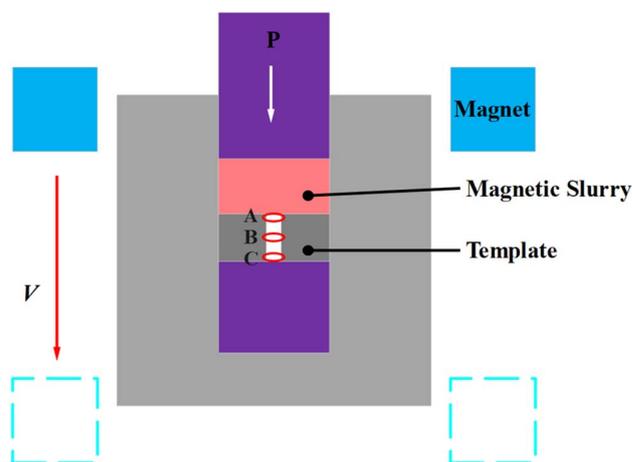

Fig. 1 Forming principles of gradient Fe_3O_4/PVDF magnetic composite.

particles in the fluid under the action of the magnetic field can be expressed as:

$$F_m = \iiint v \mu_0 M \nabla H dV_p \qquad (2)$$

$$V_p = 4/3\pi \left(\frac{d_p}{2}\right)^3 \qquad (3)$$

where μ_0 and V_p represent the vacuum permeability and volume of the magnetic particles, d_p is the diameter of the magnetic particles, and it is assumed to be 100 nm in this paper. Assuming the magnetic particles are approximately spherical and the magnetization intensity is uniform inside the particles, the magnetic susceptibility can be treated as a constant. Therefore, the relationship between the magnetization intensity of the magnetic particles and the magnetic field intensity can be further expressed as:

$$M = \frac{3\chi}{3 + \chi} H \qquad (4)$$

Hence, eqn (2) can be simplified as:

$$F_m = \mu_0 M \times \nabla H V_p = \mu_0 V_p \frac{3\chi}{3 + \chi} (H \times \nabla) H \qquad (5)$$

Therefore, the electromagnetic force acting on magnetic particles is primarily influenced by the magnetization intensity and magnetic field gradient of the particles. This paper will investigate the regulatory mechanisms of the distribution of magnetic particles and the magnetic properties of composites by designing controlled experiments to study the parameters that affect the magnetization intensity and magnetic field gradient of magnetic particles.

Table 1 presents the names, chemical formulas, and manufacturers of the primary experimental materials employed in the fabrication of Fe_3O_4/PVDF gradient magnetic composites. No additional treatments of the experimental materials are necessary throughout the experimental procedure. The self-made template used in this study was fabricated from shape memory epoxy resin using a compression molding technique. The specific fabrication process can be found in ref. 29. The template size selected for the shaping process of Fe_3O_4/PVDF magnetic composites is 1 mm wide, 2 mm deep, and 10 mm long. In order to precisely control each experimental step of the magnetic-induction mold shaping process, the forming process of the Fe_3O_4/PVDF gradient magnetic composite is divided into the following two steps:

Preparation of Fe_3O_4/PVDF magnetic slurry[30–32]

A solution mixing technique is used to prepare Fe_3O_4/PVDF magnetic slurry. First, sequentially take x g of Fe_3O_4 nanoparticles, $(10 - x)$ g of PVDF powder, and 50 mL of DMF solvent. Secondly, the weighed nanoparticles are added to DMF solvent and treated in an ultrasonic cleaner for 1 h to ensure complete dispersion of the magnetic particles. The slurry is preheated at 60 °C during this process. Then add the pre-weighed PVDF powder into it. After thorough stirring, the mixture is kept at 60 °C in a water bath for at least 3 h until a homogeneous, viscous, and black mixture slurry is obtained. Throughout the heating and insulation process, ultrasonic oscillation is continuously applied to ensure the uniform dispersion of Fe_3O_4 magnetic particles in the magnetic slurry and prevent sedimentation. In this experimental process, the amounts of Fe_3O_4 nanoparticles added were 1 g, 2 g, and 3 g respectively. For convenience in writing, the initial content of Fe_3O_4 nanoparticles is designated as 0.1, 0.2, and 0.3, respectively.

Filling of Fe_3O_4/PVDF magnetic slurry

After cleaning the template in alcohol and letting it air dry, apply dimethyl silicone oil on its surface before placing it inside the mold base. Once the template is securely sealed, 10 mL of the Fe_3O_4/PVDF magnetic slurry prepared in step (1) is slowly injected into the piston chamber using a syringe. The piston rod is then inserted into the piston cylinder and fixed in place. To fill the Fe_3O_4/PVDF slurry into the template, the hydraulic jack is continuously pressed, causing the pressure plate of the press to gradually move upward. This squeezing action helps to ensure that the slurry completely fills the template. Once the pressure gauge reaches 500 N, the pressure is maintained at that level. Next, the stepper motor of the magnetic field generator is activated, and it moves back and forth in an up-and-down motion based on the specified driving program. This movement of the magnetic field generator helps to distribute the Fe_3O_4/PVDF slurry evenly within the template during the filling experiment. The process continues until the template filling is complete. After the DMF solvent in the slurry completely evaporates, the sealing device is opened, and the filled template is carefully removed. Any remaining Fe_3O_4/PVDF magnetic slurry on the surface of the template is wiped off. Finally, the template is demolded, resulting in the formation of the Fe_3O_4/PVDF gradient magnetic composite.

Samples with a thickness of 1 mm were extracted from three different sections of the Fe_3O_4/PVDF magnetic composite: the starting end (A), middle (B), and ending end (C).

Table 1 Experimental materials used for the preparation of Fe_3O_4/PVDF magnetic composites

Material name	Chemical formula	Purity	Manufacturer
Fe_3O_4 nanoparticles	Fe_3O_4	A.R	Shanghai Chile metallurgy
PVDF	$[-CH_2-CF_2-]_n-$	A.R	Tianjin Fuyu Fine chemical Co., Ltd
DMF	C_3H_7NO	A.R	Tianjin Fuyu Fine chemical Co., Ltd
Dimethyl silicone oil	$[(CH_3)_2SiO]_n$	A.R	Tianjin Fuyu Fine chemical Co., Ltd
Template	Epoxy resin	—	Self-made

Microstructural characterization and EDS analysis of the samples were conducted using the field emission scanning electron microscope (FEI QUANTA FEG250), equipped with the EDAX element spectroscopy system. The EDS analysis was carried out in surface scanning mode. Due to the inability to measure hydrogen element content, PVDF was calibrated using carbon (C), and fluorine (F) elements, while iron (Fe) and oxygen (O) elements were used for calibration of the Fe_3O_4 magnetic nanoparticles. However, due to the incomplete evaporation of DMF solvent, there may still be residual nitrogen (N) elements. Therefore, the subsequent analysis will focus on the Fe, C, F, O and N content and distribution to investigate the impact of varying magnetic field strength, magnet spacing, initial particle content, and magnet movement speeds on the distribution state of magnetic particles in the composite material. The magnetic properties of the Fe_3O_4/PVDF composite were evaluated using the Quantum Design-PPMS 9 comprehensive physical property measurement system. The testing process was conducted at a temperature of 300 K, with a selected magnetic field strength range of −10 000 Oe to 10 000 Oe. The Bruker D8 Advance is used to test the phase composition of Fe_3O_4 magnetic nanoparticles and Fe_3O_4/PVDF composites, with a Cobalt target material. This paper defines the ratio of Fe to F element content as the parameter $R_{Fe/F}$, to characterize the variation of Fe_3O_4 nanoparticles content in Fe_3O_4/PVDF composites.

3 Results and discussions

3.1 The structure and performance of Fe_3O_4 nanoparticle

Fig. 2 presents the test results of the microstructure, X-ray diffraction (XRD), and magnetic performance of Fe_3O_4 nanoparticles. From the SEM images, it can be seen that the particle size of the magnetic particles is nearly uniform, at approximately 100 nm, consistent with the nominal value. XRD indicates that the magnetic particles consist only of the Fe_3O_4
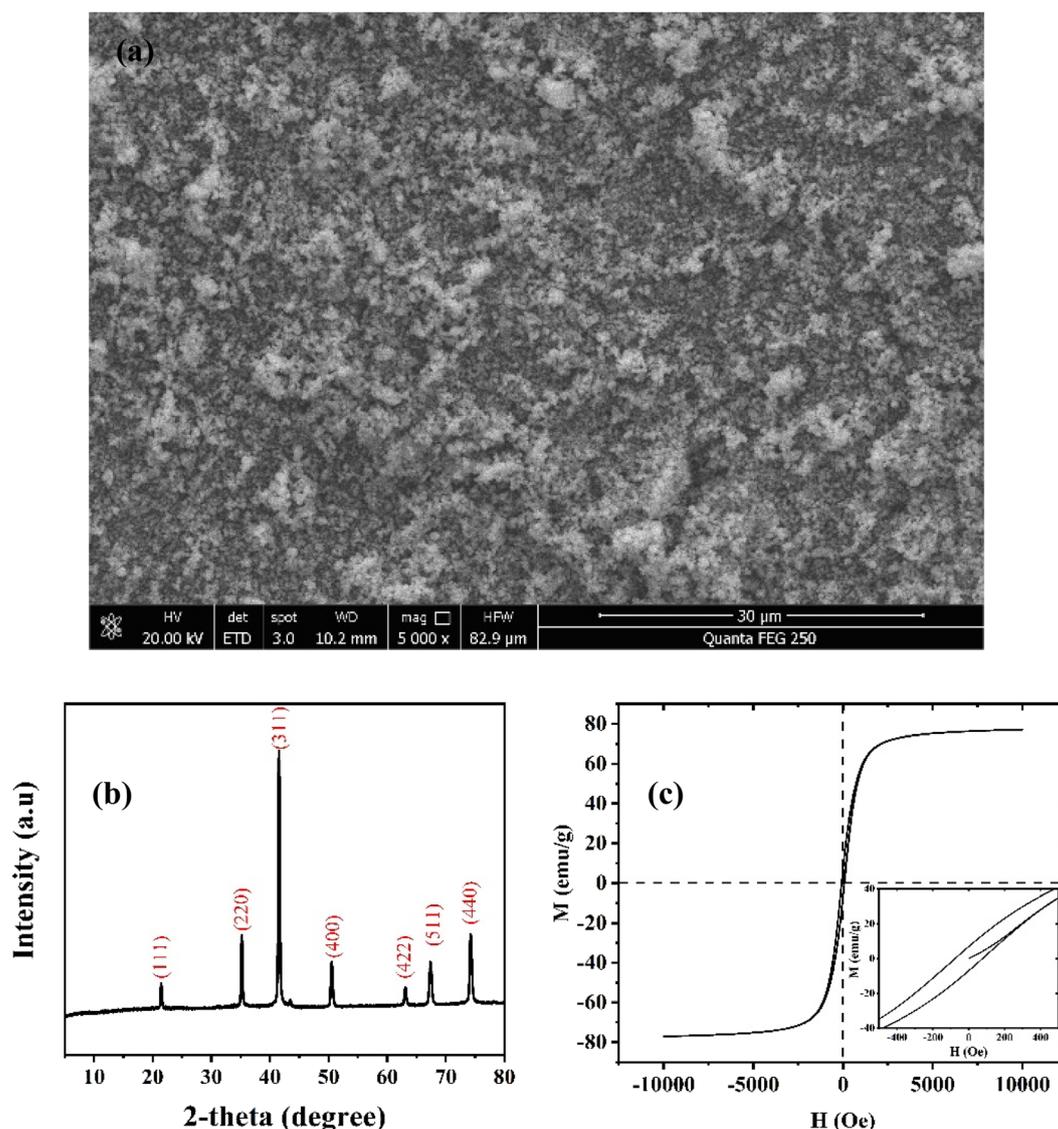

Fig. 2 The SEM image (a), XRD patterns (b), and magnetic properties (c) of Fe_3O_4 nanoparticles.

phase, and are well preserved without any signs of deterioration. The nanoparticles reach saturation at a magnetic field strength of 5000 Oe, with a saturation magnetization of 77.1 emu g^{-1}, residual magnetization of 6.9 emu g^{-1}, and coercivity of 77.7 Oe.

3.2 The structure of Fe$_3$O$_4$/PVDF composites

Fig. 3 shows the microstructure and elemental distribution of the Fe$_3$O$_4$/PVDF composite, as well as the XRD patterns. During the PVDF polymerization process, as the DMF solvent gradually evaporated. Surface tension or cohesion forces on the PVDF polymer molecule surfaces led to their continuous aggregation, ultimately forming the spherical shape observed in Fig. 3. The PVDF spheres showed nearly uniform coverage of the entire region. From the XRD patterns, it can be seen that PVDF predominantly exhibits three crystal structures, including (020), (110) and (131). The distribution of N element almost overlaps with that of C and F elements, and the ratio between N and F elements remains constant. Furthermore, EDS mapping confirmed that Fe and O elements were uniformly attached to the PVDF spheres, with the small particles observed in the SEM image representing Fe$_3$O$_4$ nanoparticles. Changing the experimental conditions only alters the content of magnetic nanoparticles without causing any change in the PVDF structure. Therefore, the variation of Fe element content in composites can be used to characterize the proportion of Fe$_3$O$_4$ nanoparticles. Considering the minor differences in the SEM morphology of the Fe$_3$O$_4$/PVDF composite, this paper will discuss the compositional gradient changes through the analysis of EDS statistical results.
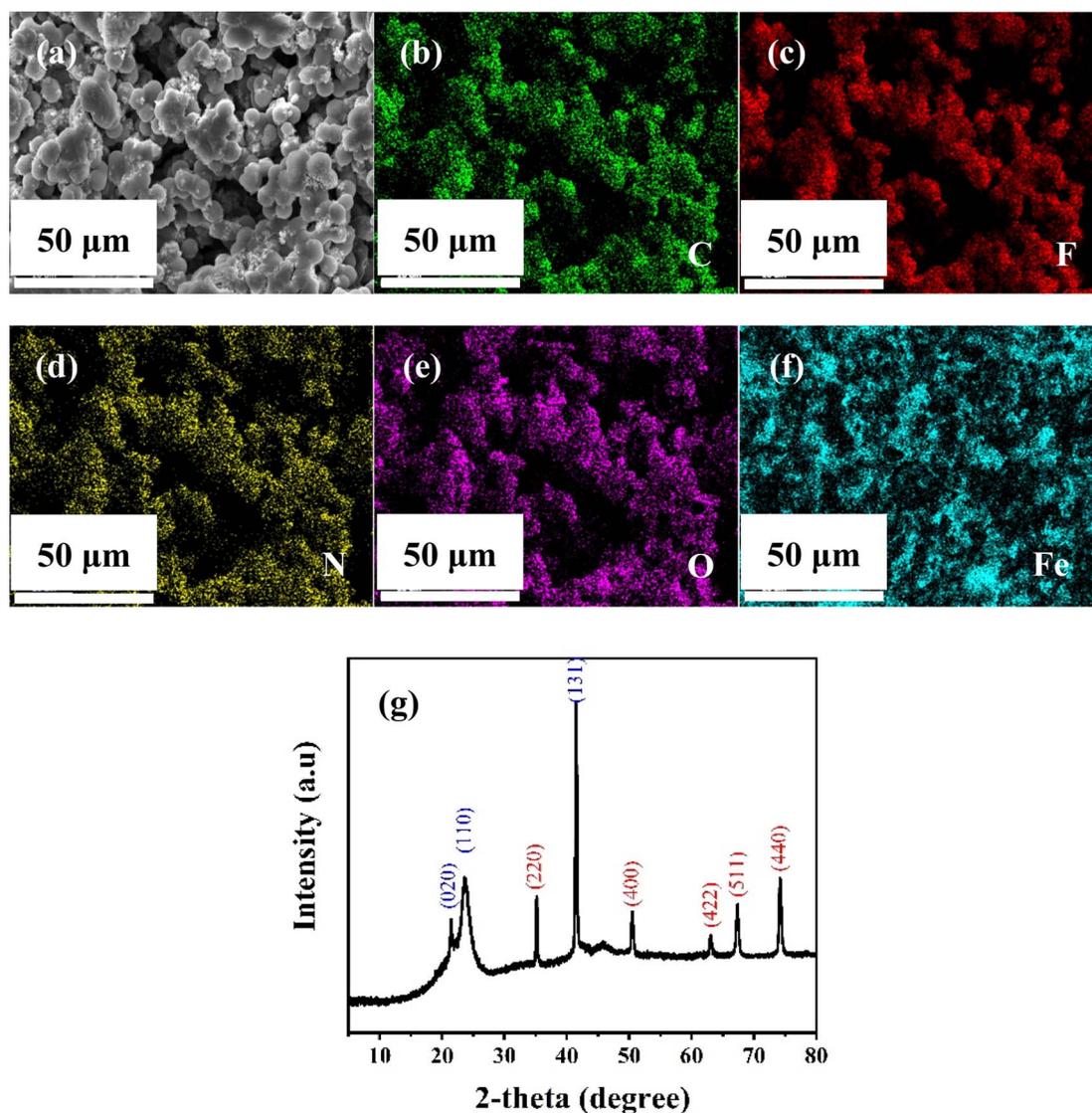

Fig. 3 (a–f) SEM-EDS mapping images of Fe$_3$O$_4$/PVDF composites prepared under the conditions of magnetic field strength 0.5 T, magnet spacing 5 mm, magnet movement speeds 1.0 mm s^{-1}, and initial particle content 0.2, showing the distribution of the constituent elements, (g) XRD patterns for Fe$_3$O$_4$/PVDF composites, in which (020), (110) and (131) correspond to PVDF, while the others correspond to Fe$_3$O$_4$ nanoparticles.

3.3 Effect of magnetic field strength on the composition and magnetic properties

Magnetic field strength plays a significant role in the electromagnetic force acting on magnetic particles. In this study, a single-variable experiment was conducted with a constant initial content of magnetic nanoparticles set at 0.2. The distance between the magnets was 5 mm, and the speed of magnet movement was 1 mm s^{-1}. Fe_3O_4/PVDF magnetic composites were prepared under magnetic field strengths of 0.35 T, 0.5 T, and 0.8 T. The highest concentration of Fe_3O_4 nanoparticles was found at the end (C) of the composite, while the lowest concentration was observed at the starting end (A). This finding directly demonstrates the effectiveness of the magnetic-assisted method for creating gradient magnetic composites. The content of Fe, C, F, O, and N elements, as well as the parameter $R_{Fe/F}$, in Fe_3O_4/PVDF magnetic composites prepared under different magnetic field strengths can be found in Table S1.† As the magnetic field strength increased from 0.35 T to 0.5 T and 0.8 T, the initial $R_{Fe/F}$ in the starting end (A) decreased from 0.466 to 0.378 and 0.336, respectively. In contrast, the $R_{Fe/F}$ in the ending end (C) increased from 1.028 to 1.447 and 2.563, respectively. Thus, the gradient of Fe_3O_4 nanoparticles between the starting end (A) and ending end (C) of the Fe_3O_4/PVDF composite

increased with the magnetic field strength. It is important to note that with a magnetic field strength of 0.8 T, Fe_3O_4 nanoparticles primarily accumulated in the starting end (A) during the initial stage of magnet movement. However, they subsequently moved downwards due to the electromagnetic force exerted during the magnet movement process. Therefore, the final result still followed the pattern of lower nanoparticle content in the starting end (A) and higher particle content in the ending end (C). However, the concentration of Fe element in the starting end (A) of the Fe_3O_4/PVDF composite was higher than that in the middle (B).

This study aimed to investigate the impact of variations in magnetic field strength on the gradient of the Fe_3O_4/PVDF composite. By examining samples extracted from three different positions of the composite (starting end A, middle B, and ending end C), the magnetic properties were characterized, as shown in Fig. 4. The results revealed that the magnetization of the Fe_3O_4/PVDF composite reached saturation within the range of −10 000 Oe to 10 000 Oe magnetic field strength, indicating that the composite is a soft magnetic material. The magnetic properties of the composite exhibited gradual improvement along the direction of the magnetic field movement, as a result of the magnetic orientation motion of the Fe_3O_4 nanoparticles.
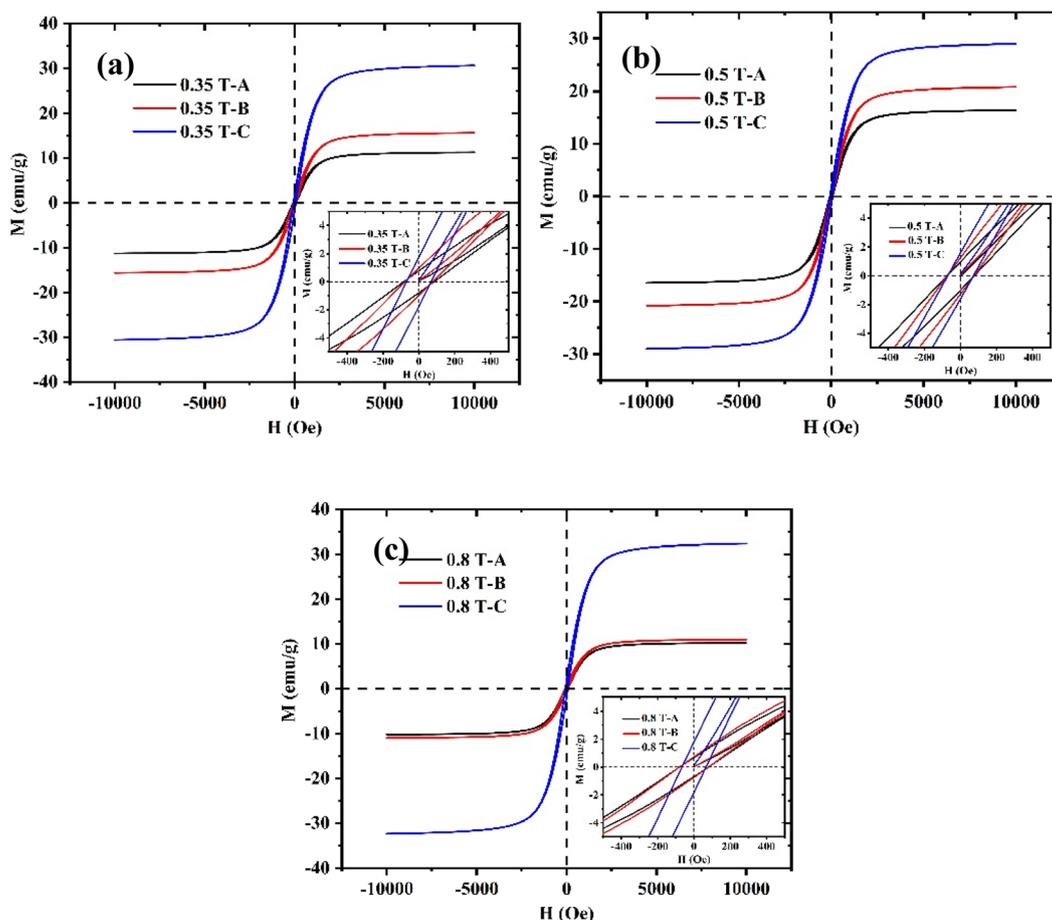

Fig. 4 The influence of magnetic field strength variation on the magnetic properties of Fe_3O_4/PVDF composite at A, B, and C: (a) $B = 0.35$ T, (b) $B = 0.5$ T, (c) $B = 0.8$ T.

Notably, the ending end C displayed the strongest magnetic performance, while the starting end A exhibited the weakest. To quantify the magnetic performance parameters of the composite, the study extracted the coercive force (H_c), remanent magnetization (M_r), and saturation magnetization (M_s) from the hysteresis loops, as shown in Table 2. The saturation magnetization and remanent magnetization gradually increased from the starting end A to the ending end C due to the aggregation of Fe_3O_4 nanoparticles under the influence of the magnetic field. However, the coercive force did not exhibit a consistent variation as it is affected by factors like material grain boundaries and dislocations.[33] Additionally, increasing the magnetic field strength from 0.35 T to 0.5 T and 0.8 T resulted in an increment in the saturation magnetization of the ending end C and a decrement in the saturation magnetization of the starting end A. This suggests that the magnetic gradient between the starting A and ending C ends of the composite decreased with higher magnetic field strength. It is important to note that, at a magnetic field strength of 0.8 T, the saturation magnetization of the starting end A surpassed that of the middle B, indicating a variation in the content of Fe_3O_4 nanoparticles.

3.4 Effect of magnet spacing on the composition and magnetic properties

The distance between two magnets directly affects the distribution of the magnetic field in the template filling region. In this study, Fe_3O_4/PVDF composites were prepared by keeping a constant initial content of Fe_3O_4 nanoparticles at 0.2, a magnetic field strength of 0.35 T, and a magnet movement speed of 1 mm s^{-1}, with magnet spacings of 5 mm, 7 mm, and 9 mm. The content of Fe, C, F, O, and N elements, as well as the parameter $R_{Fe/F}$, in Fe_3O_4/PVDF magnetic composites prepared under different magnet spacings can be found in Table S2.† For magnet spacings of 7 mm and 9 mm, the parameter $R_{Fe/F}$ at the starting end (A) of the Fe_3O_4/PVDF composite is recorded as 0.445 and 0.663 respectively. In the middle section (B), the parameter $R_{Fe/F}$ is measured as 0.64 and 0.728 respectively, while at the ending end (C) it is found to be 1.389 and 1.026 respectively. Comparative analysis reveals that the Fe_3O_4 nanoparticles content is highest at the ending end (C) of the Fe_3O_4/PVDF composite when the magnet spacing is 7 mm, with the largest gradient of magnetic nanoparticle content observed

between both ends. This is because the formation process of the Fe_3O_4/PVDF gradient magnetic composite requires a balance between magnetic field strength and its gradient for optimal results. As the magnet distance increases from 5 mm to 7 mm, the spatial magnetic field strength in the template filling region decreases, but the magnetic field gradient in the direction of magnet movement increases. However, when the magnet distance further increases to 9 mm, the decrease in spatial magnetic field strength outweighs the increase in magnetic field gradient. Therefore, compared to magnet spacings of 5 mm and 9 mm, a magnet spacing of 7 mm is more advantageous in enhancing the gradient of Fe_3O_4 nanoparticle content between the starting (A) and ending (C) ends of the Fe_3O_4/PVDF composite. These observations suggest that manipulating magnet distances during the preparation of Fe_3O_4/PVDF composites is crucial in determining the spatial distribution and content of Fe_3O_4 nanoparticles within the material. These findings highlight the importance of optimizing the magnetic field effect to achieve the desired characteristics.

The magnetic performance of the Fe_3O_4/PVDF composite at three different positions: the starting end (A), the middle (B), and the ending end (C), under various magnet spacing conditions, is shown in Fig. 5. Meanwhile, the statistical results for the coercive force (H_c), remanence (M_r), and saturation magnetization (M_s) of the Fe_3O_4/PVDF composite extracted from the hysteresis loops are presented in Table 3. Notably, as the magnet spacing varies, the saturation magnetization and remanence of the Fe_3O_4/PVDF composite gradually increase from the starting end (A) to the ending end (C), while the coercive force does not demonstrate a consistent pattern. For example, when the magnet spacing increases from 5 mm to 7 mm, the saturation magnetization of the Fe_3O_4/PVDF composite at the ending end (C) increases from 27.2 emu g^{-1} to 30.3 emu g^{-1}, and the remanence rises from 1.5 emu g^{-1} to 1.6 emu g^{-1}. In contrast, the saturation magnetization at the starting end (A) decreases from 16.4 emu g^{-1} to 15.6 emu g^{-1}. However, with a further increase in magnet spacing to 9 mm, the saturation magnetization at the starting (A) and ending (C) ends of the Fe_3O_4/PVDF composite becomes 19.0 emu g^{-1} and 25.8 emu g^{-1}, respectively, with corresponding remanence values of 1.1 emu g^{-1} and 1.5 emu g^{-1}. The magnetic gradient between the starting (A) and ending (C) ends of the Fe_3O_4/PVDF composite follows an increasing-then-decreasing trend with the change in magnet spacing, which is consistent with the fluctuation in the content of Fe_3O_4 nanoparticles. Consequently, it is advisable to avoid excessively large magnet spacing in practical applications to maintain optimal magnetic performance.

3.5 Effect of magnet movement speeds on the composition and magnetic properties

The y-component of the electromagnetic force is the primary driving force for the magnetically-induced movement of Fe_3O_4 nanoparticles. This force is directly proportional to the gradient of the magnetic field strength in the y-direction and the strength of magnetization of the nanoparticles, as described by eqn (2). Increasing the speed of magnet movement does not

Table 2 H_c, M_r, and M_s of Fe_3O_4/PVDF composite at A, B, and C under different magnetic field strengths

Items	H_c (Oe)	M_r (emu g^{-1})	M_s (emu g^{-1})
0.35 T-A	75.4	1.0	16.4
0.35 T-B	72.1	1.4	23.7
0.35 T-C	68.0	1.5	27.2
0.5 T-A	62.7	0.8	14.5
0.5 T-B	66.1	1.2	22.2
0.5 T-C	71.1	1.6	29.0
0.8 T-A	79.1	0.8	11.0
0.8 T-B	78.9	0.7	10.2
0.8 T-C	73.1	1.9	33.7

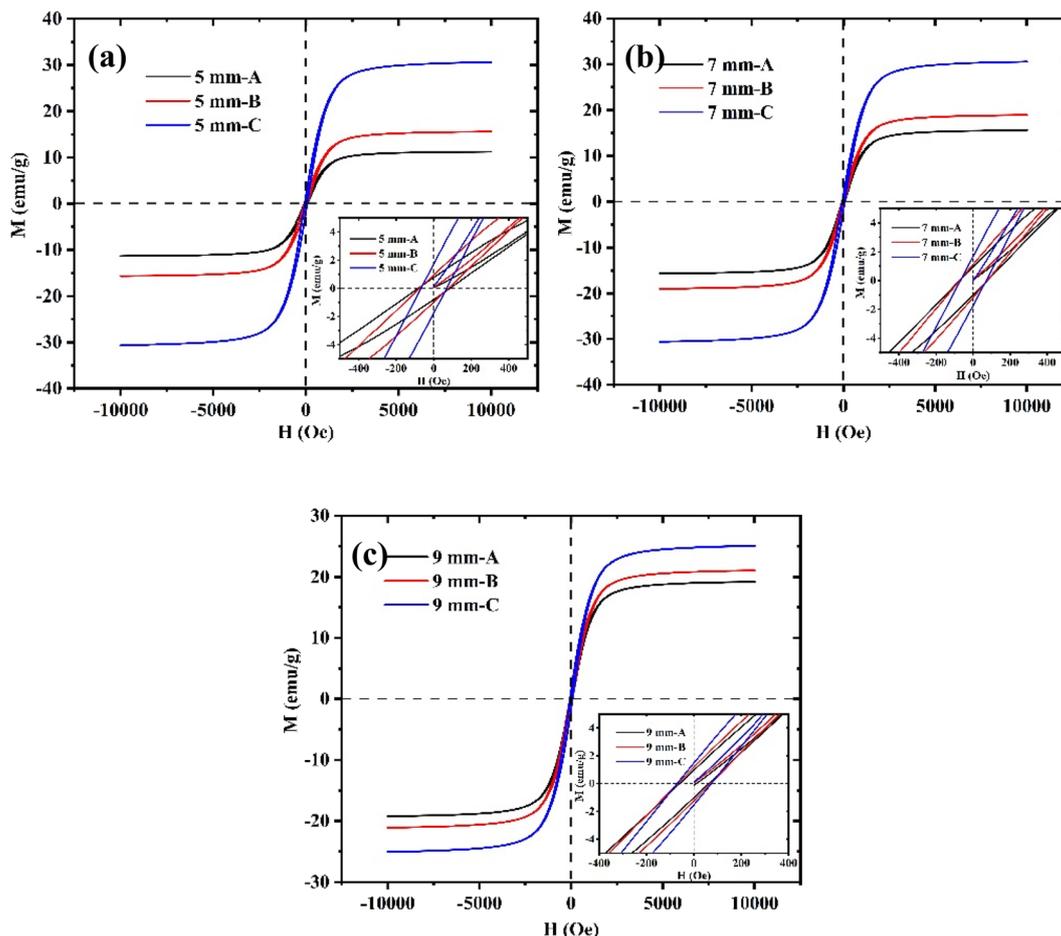**Fig. 5** Influence of magnet spacing variation on the magnetic properties of Fe_3O_4/PVDF composite at A, B, and C: (a) 5 mm, (b) 7 mm, (c) 9 mm.

Table 3 H_c, M_r, and M_s of Fe_3O_4/PVDF composites at A, B, and C under different magnet spacing conditions

Items	H_c (Oe)	M_r (emu g^{-1})	M_s (emu g^{-1})
5 mm-A	75.4	1.0	16.4
5 mm-B	72.1	1.4	23.7
5 mm-C	67.9	1.5	27.2
7 mm-A	77.0	1.0	15.6
7 mm-B	77.4	1.1	17.0
7 mm-C	69.5	1.6	30.3
9 mm-A	74.4	1.1	19.0
9 mm-B	74.6	1.3	20.8
9 mm-C	72.3	1.5	25.8

affect the spatial distribution of the magnetic field but it does increase the gradient of the y-component of the magnetic field intensity. As a result, the y-component of the electromagnetic force acting on the Fe_3O_4 nanoparticles also increases. However, increasing the speed of magnet movement also significantly reduces the effective interaction time between the electromagnetic force and the magnetic nanoparticles. This shortened interaction time has two opposing effects on the distribution of the Fe_3O_4 nanoparticles. On one hand, the increased gradient of the y-component of the magnetic field intensity enhances the

movement of the particles. On the other hand, the shortened interaction time decreases the tendency of the Fe_3O_4 nanoparticles to aggregate downwards. To enhance the magnetic gradient at both ends of the Fe_3O_4/PVDF composite, it is essential to select the appropriate speed of magnet movement. By carefully choosing the magnet movement speeds, a balance can be achieved between the increased gradient of the y-component of the magnetic field intensity and the shortened interaction time, leading to an improved magnetic gradient.

This study maintains a constant initial content of Fe_3O_4 nanoparticles at 0.2, magnetic field strength at 0.35 T, and the distance between the two magnets at 5 mm. The Fe_3O_4/PVDF composites were prepared under different magnet movement speeds of 0.5 mm s^{-1}, 1.0 mm s^{-1}, and 1.5 mm s^{-1}. The content of Fe, C, F, O, and N elements, as well as the parameter $R_{Fe/F}$, in Fe_3O_4/PVDF magnetic composites prepared under different magnet movement speeds can be found in Table S3.† At magnet movement speeds of 0.5 mm s^{-1} and 1.5 mm s^{-1}, the parameter $R_{Fe/F}$ at the starting end (A) of the Fe_3O_4/PVDF composite is 0.457 and 0.539, respectively. In the middle (B), it is 0.798 and 0.791, while at the ending end (C) they are 1.407 and 1.174, respectively. The increase in magnet movement speed enhances the gradient of the y-component of the magnetic field strength
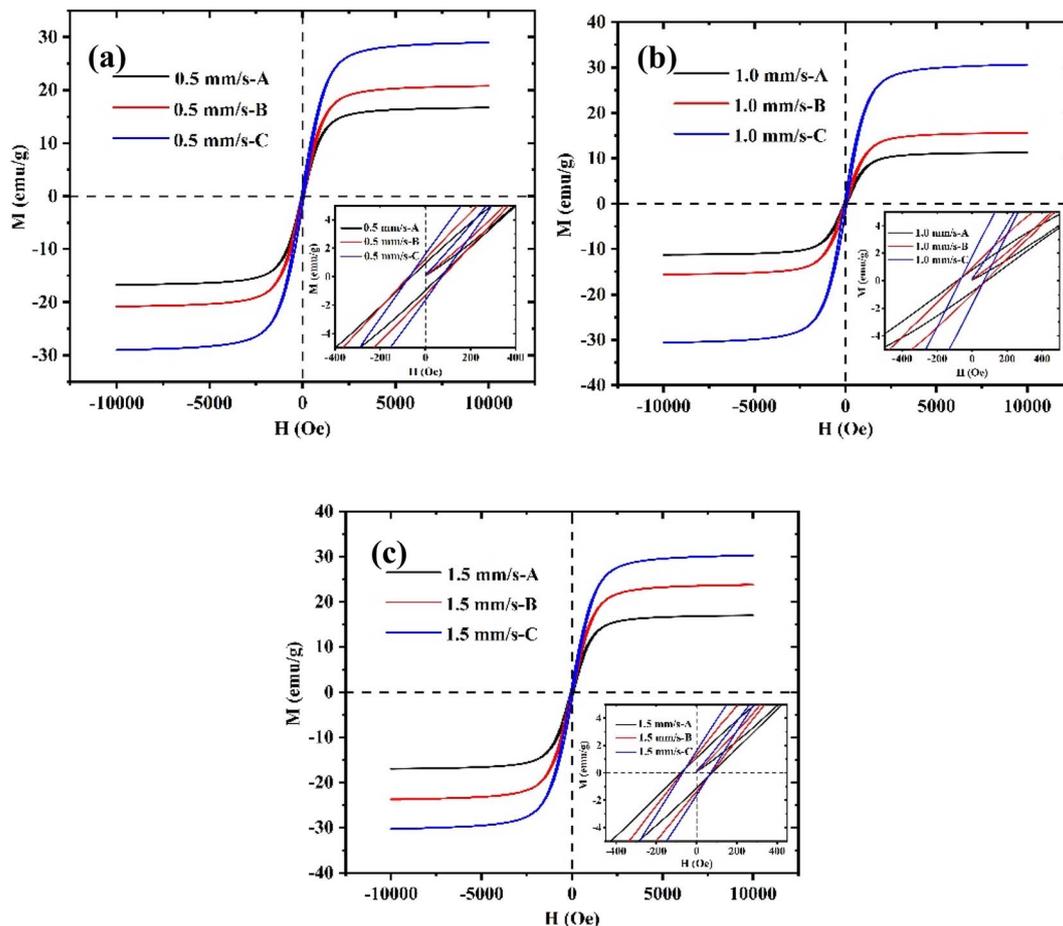
Fig. 6 Influence of magnet movement speed on the magnetic properties of Fe_3O_4/PVDF composite at A, B, and C: (a) 0.5 mm s^{-1}, (b) 1.0 mm s^{-1}, (c) 1.5 mm s^{-1}.

in space but reduces the interaction time between the Fe_3O_4 nanoparticles and the electromagnetic force. Consequently, as the magnet movement speed increases from 0.5 mm s^{-1} to 1.0 mm s^{-1}, the movement of the magnetic nanoparticles is primarily promoted by the increased gradient of the y-component of the magnetic field strength. However, with a further increase to 1.5 mm s^{-1}, the inhibitory effect of the shortened interaction time of the electromagnetic force counteracts the tendency of Fe_3O_4 nanoparticles to aggregate downwards. As a result, the Fe_3O_4 nanoparticles content in the ending end (C) of the Fe_3O_4/PVDF composite is at its maximum at a magnet movement speed of 1.5 mm s^{-1}, at its minimum at a magnet movement speed of 1.0 mm s^{-1}, and the magnetic nanoparticles content gradient between the starting (A) and ending (C) ends of the Fe_3O_4/PVDF composite is highest at a speed of 0.5 mm s^{-1}. Therefore, compared to magnet movement speeds of 0.5 mm s^{-1} and 1.5 mm s^{-1}, a magnet movement speed of 1.0 mm s^{-1} is more conducive to improving the Fe_3O_4 nanoparticle content gradient between the starting (A) and ending (C) ends of the Fe_3O_4/PVDF composite.

The results of the magnetic characterization of the Fe_3O_4/PVDF composite at three different points, namely the starting end (A), middle (B), and ending end (C), under varying magnet

movement speed are shown in Fig. 6. Table 4 provides the extracted coercive force (H_c), residual magnetization (M_r), and saturation magnetization (M_s) of the composite based on the hysteresis loops. From the analysis, it was observed that the M_r and M_s of the composite increased from the starting to the ending end at different magnet movement speed. For magnet movement speed ranging from 0.5 mm s^{-1} to 1.0 mm s^{-1}, the saturation magnetization at the ending end (C) decreased from 29.0 emu g^{-1} to 27.2 emu g^{-1}, and the residual magnetization

Table 4 H_c, M_r, and M_s of Fe_3O_4/PVDF magnetic composite at A, B, and C under different magnet movement speeds

Items	H_c (Oe)	M_r (emu g^{-1})	M_s (emu g^{-1})
0.5 mm s^{-1}-A	75.1	1.0	15.7
0.5 mm s^{-1}-B	70.6	1.3	22.8
0.5 mm s^{-1}-C	71.1	1.6	29.0
1.0 mm s^{-1}-A	75.4	1.0	16.4
1.0 mm s^{-1}-B	72.1	1.4	23.7
1.0 mm s^{-1}-C	67.9	1.5	27.2
1.5 mm s^{-1}-A	62.4	1.0	16.7
1.5 mm s^{-1}-B	71.2	1.3	23.8
1.5 mm s^{-1}-C	68.6	1.8	30.6

also decreased from 1.6 emu g^{-1} to 1.5 emu g^{-1}. However, the saturation magnetization at the starting end (A) increased from 15.7 emu g^{-1} to 16.4 emu g^{-1}. At a magnet movement speed of 1.5 mm s^{-1}, the saturation magnetization at the starting (A) and ending (c) ends of the composite material are 16.7 emu g^{-1} and 30.6 emu g^{-1}, respectively. Likewise, the residual magnetization at the starting and ending ends is 0.9 emu g^{-1} and 1.8 emu g^{-1}, respectively. The magnetic gradient between the starting (A) and ending (C) ends of the Fe$_3$O$_4$/PVDF composite under the three magnet movement speeds should be arranged in descending order as follows: 1.5 mm s^{-1} > 0.5 mm s^{-1} > 1.0 mm s^{-1}. To improve the magnetic gradient between the starting (A) and ending (C) ends of the Fe$_3$O$_4$/PVDF composite, it is suggested to increase either the amplitude or the acting time of the electromagnetic force on the Fe$_3$O$_4$ nanoparticles. Consequently, when selecting the magnet movement speed, it is not necessary to consider both the acting time and amplitude of the electromagnetic force simultaneously.

3.6 Effect of the initial content on the composition and magnetic properties

The greater the initial content of Fe$_3$O$_4$ nanoparticles, the stronger the electromagnetic force experienced by the magnetic slurry during the template filling process. To examine the influence of the initial magnetic particle content on the microstructure and magnetic properties, this study held the magnetic field strength at 0.35 T, the magnet spacing at 5 mm, and the magnet movement speed at 1 mm s^{-1} constant while preparing Fe$_3$O$_4$/PVDF composites with initial magnetic nanoparticle contents of 0.1, 0.2, and 0.3, respectively. The content of Fe, C, F, O, and N elements, as well as the parameter $R_{Fe/F}$, in Fe$_3$O$_4$/PVDF magnetic composites prepared under different magnet movement speeds can be found in Table S4.† Specifically, with Fe$_3$O$_4$ nanoparticles content at 0.1 and 0.3, the parameter $R_{Fe/F}$ at the starting end (A) of the Fe$_3$O$_4$/PVDF composite is 0.342 and 0.711, in the middle (B) is 0.645 and 1.002, and at the ending ends (C) they are 0.738 and 1.645, respectively. As the initial content of Fe$_3$O$_4$ nanoparticles increases from 0.1 to 0.2 and 0.3, the Fe$_3$O$_4$ nanoparticles content at the ending ends (C) of the Fe$_3$O$_4$/PVDF composite gradually rises, while the content of Fe$_3$O$_4$ nanoparticles at the starting end (A) gradually decreases. Furthermore, the gradient of magnetic nanoparticle content between the starting (A) and ending (C) ends of the composite gradually increases. Therefore, selecting a higher initial content of Fe$_3$O$_4$ nanoparticles is more advantageous in enhancing the gradient of magnetic nanoparticles content between the starting (A) and ending (C) ends of the Fe$_3$O$_4$/PVDF composite.
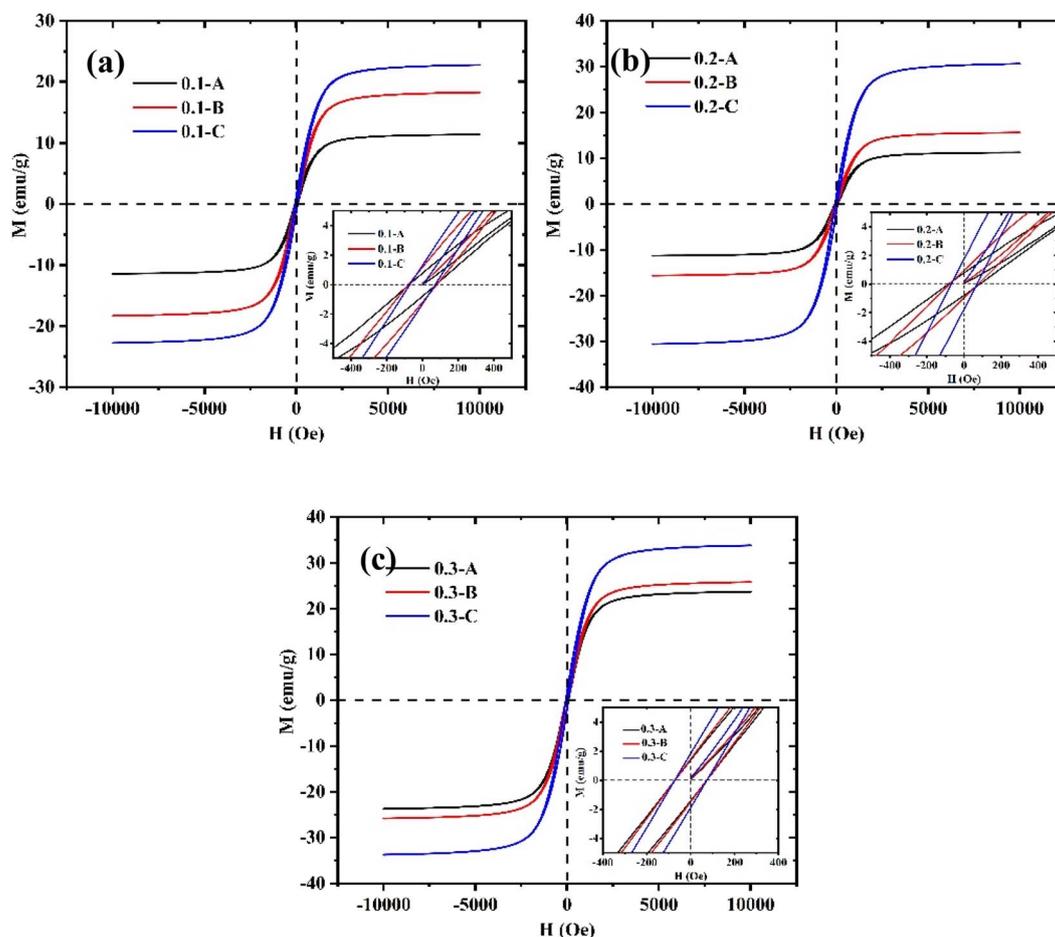

Fig. 7 Influence of initial particle content variation on the magnetic properties of Fe$_3$O$_4$/PVDF composite at A, B, and C: (a) 0.1, (b) 0.2, (c) 0.3.

Table 5 H_c, M_r, and M_s of Fe_3O_4/PVDF magnetic composites at A, B, and C under different initial particle content conditions

Items	H_c (Oe)	M_r (emu g^{-1})	M_s (emu g^{-1})
0.1 A	75.1	0.8	11.4
0.1-B	79.6	1.2	18.3
0.1-C	70.1	1.2	21.1
0.2-A	75.4	1.0	16.4
0.2-B	72.1	1.4	23.7
0.2-C	67.9	1.5	27.2
0.3-A	61.7	1.0	19.2
0.3-B	72.2	1.5	25.1
0.3-C	66.2	1.8	32.4

Fig. 7 illustrates the magnetic properties of the Fe_3O_4/PVDF composite at different positions within the composite – the starting end (A), middle (B), and ending end (C) – under various initial Fe_3O_4 nanoparticles content conditions. Based on the obtained hysteresis loops, the coercivity (H_c), residual magnetization (M_r), and saturation magnetization (M_s) of the composite were determined, and the statistical results are presented in Table 5. The data indicates that as the initial Fe_3O_4 nanoparticle content increases, the M_r and M_s of the Fe_3O_4/PVDF composite progressively rise from the starting end (A) to the ending end (C). Specifically, as the initial nanoparticles content increases from 0.1 to 0.2 and 0.3, the lower part of the Fe_3O_4/PVDF composite shows an increase in saturation magnetization from 21.1 emu g^{-1} to 27.2 emu g^{-1} and 32.4 emu g^{-1}, and an increase in residual magnetization from 1.2 emu g^{-1} to 1.5 emu g^{-1} and 1.8 emu g^{-1}. Similarly, the starting end demonstrates a rise in saturation magnetization from 11.4 emu g^{-1} to 16.4 emu g^{-1} and 19.2 emu g^{-1}. Therefore, a higher initial Fe_3O_4 nanoparticle content within the range of 0.1–0.3 creates a greater magnetic gradient between the starting (A) and ending (C) ends of the Fe_3O_4/PVDF composite.

4 Conclusions

This study employs the magnetic-assisted template method to fabricate Fe_3O_4/PVDF gradient magnetic composites and investigates the impact of parameters including magnetic field strength, magnet spacing, initial content, and magnet movement speed on the distribution of Fe_3O_4 nanoparticles through structural and magnetic performance characterization. The findings reveal that increasing the magnetic field intensity from 0.35 T to 0.5 T and 0.8 T results in a rise in the saturation magnetization gradient between the starting (A) and ending (C) ends of the composite, from 10.7 emu g^{-1} to 14.5 emu g^{-1} and 22.8 emu g^{-1}, respectively. Therefore, a higher magnetic field intensity proves more advantageous in enhancing the magnetic property gradient of the composite. In the case of magnet spacing, namely 5 mm, 7 mm, and 9 mm, the saturation magnetization gradient between the starting (A) and ending (C) ends of the composite is 10.7 emu g^{-1}, 14.7 emu g^{-1}, and 6.9 emu g^{-1}, respectively. Similarly, at magnet movement speeds of 0.5 mm s^{-1}, 1.0 mm s^{-1}, and 1.5 mm s^{-1}, the

saturation magnetization gradient between the starting (A) and ending (C) ends of the composite is 13.3 emu g^{-1}, 10.7 emu g^{-1}, and 13.9 emu g^{-1}, respectively. Furthermore, raising the initial content of magnetic particles from 0.1 to 0.2 and 0.3 leads to an increase in the saturation magnetization gradient between the starting (A) and ending (C) ends of the composite, from 9.7 emu g^{-1} to 10.7 emu g^{-1} and 13.2 emu g^{-1}, respectively. Hence, a higher initial content of magnetic particles carries benefits for enhancing the magnetic property gradient of the composite. Overall, the magnetic properties of the Fe_3O_4/PVDF composite can be adjusted by controlling parameters such as magnetic field strength, magnet spacing, initial content of magnetic nanoparticles, and magnet movement speed.

Conflicts of interest

The authors declare that they have no conflict of interests.

References

1 K. Wang, F. B. Zhang, K. X. Xu, Y. J. Che, M. Y. Qi and C. Song, Modified magnetic chitosan materials for heavy metal adsorption: a review, *RSC Adv.*, 2023, **13**, 6713–6736.

2 Z. H. Qian, J. Ji, L. Y. Qian, Y. X. Mao, S. C. Yao, J. Y. Xu and L. C. Wang, Interlayer coupling controlled electronic and magnetic properties of two-dimensional VOCl$_2$/PtTe$_2$ van der Waals heterostructure, *RSC Adv.*, 2023, **13**, 35018–35025.

3 A. V. Papavasileiou, M. Menelaou, K. J. Sarkar, Z. Sofer, L. Polavarapu and S. Mourdikoudis, Ferromagnetic elements in two-dimensional materials: 2D magnets and beyond, *Adv. Funct. Mater.*, 2023, **32**, 2309046.

4 A. Sundaresan and C. N. R. Rao, Ferromagnetism as a universal feature of inorganic nanoparticles, *Nano Today*, 2009, **4**, 96–106.

5 M. D. Nguyen, H. V. Tran, S. J. Xu and T. R. Lee, Fe_3O_4 nanoparticles: structures, synthesis, magnetic properties, surface functionalization, and emerging applications, *Appl. Sci.*, 2021, **11**, 11301.

6 L. S. Ganapathe, M. A. Mohamed, R. M. Yunus and D. D. Berhanuddin, Magnetite (Fe_3O_4) nanoparticles in biomedical application: from synthesis to surface functionalization, *Magnetochemistry*, 2020, **6**, 68.

7 M. Natali, S. Tamburini, R. Bertani, D. Desideri, M. Mozzon, D. Pavarin, F. Spizzo, L. Del Bianco, F. Zorzi and P. Sgarbossa, Novel magnetic inorganic composites: synthesis and characterization, *Polymers*, 2021, **13**, 1284.

8 Q. Lu, K. Choi, J. D. Nam and H. J. Choi, Magnetic polymer composite particles: Design and magnetorheology, *Polymers*, 2021, **13**, 512.

9 J. Wang, W. Xiong, L. Huang, Y. X. Li, Z. L. Zuo, X. Y. Hu, T. Wang, J. Q. Xiao and J. Hu, Electrochemical synthesis of core-shell Co-Ni nanorod arrays with facilely regulated magnetic properties, *Physica B*, 2019, **567**, 113–117.

10 Q. S. Zhu, R. J. Tang, F. Peng, S. C. Xu, G. Q. Liang, R. Zhao, Y. Fang, L. You and X. D. Su, Mechanical regulation of the magnetic properties of uniaxial anisotropic hexaferrite thin films, *Phys. Rev. Appl.*, 2021, **16**, 054006.

11 Z. B. Li, Y. Li, Z. X. Zhang, Y. L. Liu, Y. F. Li and X. F. Zhang, Improving magnetic properties in mischmetal-based sintered composite magnets by regulating element distribution, *AIP Adv.*, 2019, **9**, 075109.

12 Y. B. Dong, L. Zhu, B. Yin, X. R. Zhu and D. F. Li, Regulating the magnetic properties of seven-coordinated Dy (III) single-ion magnets through the effect of positional isomers on axial crystal-field, *Dalton Trans.*, 2021, **50**, 17328–17337.

13 Z. F. Shang, M. Yue, Y. Q. Li, D. T. Zhang, Z. H. Xie and Y. Q. Wang, The effect of multi-scale Cu distribution regulation on magnetic properties of Sm (CoFeCuZr)$_z$ magnets, *J. Magn. Magn. Mater.*, 2020, **502**, 166484.

14 C. Vives, Crystallization of aluminum alloys in the presence of vertical electromagnetic force fields, *J. Cryst. Growth*, 1997, **173**, 541–549.

15 J. A. Gavira and J. M. García-Ruiz, Effects of a magnetic field on lysozyme crystal nucleation and growth in a diffusive environment, *Cryst. Growth Des.*, 2009, **9**, 2610–2615.

16 L. Hu, X. Y. Feng, L. Z. Wei, K. J. Zhang, J. M. Dai, Y. C. Wu and Q. Q. Chen, MoS_2 ultrathin nanosheets obtained under a high magnetic field for lithium storage with stable and high capacity, *Nanoscale*, 2015, **7**, 10925–10930.

17 M. Y. Zhu, Y. M. Hu, Y. Li, H. M. Jin and Z. Z. Zhu, Effect of magnetic field on phase morphology transformation of MnO_2 nanostructures in a hydrothermal process, *Phys. Status Solidi C*, 2012, **9**, 122–127.

18 D. Hippo, Y. Nakamine, K. Urakawa, Y. Tsuchiya, H. Mizuta, N. Koshida and S. Oda, Formation mechanism of 100 nm-scale periodic-structures in silicon using magnetic-field-assisted anodization, *Jpn. J. Appl. Phys.*, 2008, **47**, 7398–7402.

19 K. Cui, G. Song, W. Wang, H. Liu, Y. Yang, C. Sun, Z. Zhao, H. Lin and D. Chen, Force analysis and distribution evolution of Fe_3O_4 nanoparticles in magnetic fluids, *Chin. J. Phys.*, 2024, **88**, 982–990.

20 Y. Shi, B. X. Lei, Y. K. Wang and J. J. Ye, An analytical model for the self-bias magnetoelectric effect of magnetization-graded magnetoelectric composites, *Compos. Struct.*, 2022, **300**, 116164.

21 C. I. da Silva, M. R. O. Cunha, A. Q. Barbosa, R. J. C. Carbas, E. A. S. Marques and L. F. M. da Silva, Functionally graded adhesive joints using magnetic microparticles with a polyurethane adhesive, *J. Adv. Joi. Process.*, 2021, **3**, 100048.

22 T. Mazur, L. Mazur, M. Borkowski, T. Kuciel and M. L. Szuwarzy, Polymer-nanoparticle thin scaffolds with any-shape magnetic field gradients, *Colloids Surf., A*, 2023, **677**, 132413.

23 N. N. Phuoc and C. K. Ong, Positive temperature dependence of magnetic anisotropy in NiFeW thin films fabricated by gradient composition sputtering, *Mater. Res. Express*, 2017, **4**, 076108.

24 M. Cabo, E. Pellicer, E. Rossinyol, M. Estrader, A. López-Ortega, J. Nogués, O. Castell, S. Suriñach and M. D. Baró, Synthesis of compositionally graded nanocast NiO/$NiCo_2O_4$/Co_3O_4 mesoporous composites with tunable magnetic properties, *J. Mater. Chem.*, 2010, **20**, 7021–7028.

25 X. X. Zhong, N. N. Phuoc, W. T. Soh, C. K. Ong, L. Peng and L. Z. Li, Tailoring the magnetic properties and thermal stability of $FeSiAl-Al_2O_3$ thin films fabricated by hybrid oblique gradient-composition sputtering, *J. Magn. Magn. Mater.*, 2017, **429**, 52–59.

26 H. L. Du, D. R. Cao, X. M. Chu, X. M. Liu, Z. Wen, R. C. Sun, Y. Y. Dai, S. D. Li and S. S. Yan, Tuning microwave magnetic properties of composition gradient FeCoB/Ru/FeCoB trilayer films, *J. Magn. Magn. Mater.*, 2018, **458**, 200–203.

27 P. Rabu and M. Drillon, Layered organic-inorganic materials: A way towards controllable magnetism, *Adv. Eng. Mater.*, 2003, **5**, 189–210.

28 V. Gatard, J. Deseure and M. Chatenet, Use of magnetic fields in electrochemistry: A selected review, *Curr. Opin. Electrochem.*, 2020, **23**, 96–105.

29 M. Wang and Z. M. Zhang, Research on the forming and demolding process of shape memory self-demolding mold, *AIP Adv.*, 2024, DOI: 10.1063/5.0193754.

30 K. Cui, Y. Cao, Y. C. Yang, G. H. Song, Z. L. Zhao and H. L. Lin, Enhancing magnetic properties of Ni_3Si/Fe_3O_4@PVDF composites *via* lamellar Ni_3Si template fabrication under pulsed magnetic fields, *Appl. Phys. A: Mater. Sci. Process.*, 2023, **129**, 729.

31 K. Cui, L. Yuan and Z. Zhao, Magnetic properties of Ni_3Si/Fe_3O_4@PVDF composites with different Fe_3O_4 nanoparticles content based on lamellar Ni_3Si template, *Mater. Sci. Eng., B*, 2023, **290**, 116330.

32 K. Cui, L. Yuan and Z. Zhao, Characterization and regulation of Ni_3Si//Fe_3O_4@PVDF magnetoelectric composites, *J. Magn. Magn. Mater.*, 2022, **563**, 169972.

33 G. P. Zhao, L. Zhao, L. C. Shen, J. Zou and L. Qiu, Coercivity mechanisms in nanostructured permanent magnets, *Chin. Phys. B*, 2019, **28**, 077505.